Earth, Planets and Space

FULL PAPER Open Access

Periodic oscillations of Doppler frequency excited by the traveling ionospheric disturbances associated with the Tonga eruption in 2022

Hiroyuki Nakata[1*], Keisuke Hosokawa[2], Susumu Saito[3], Yuichi Otsuka[4] and Ichoro Tomizawa[2]

Abstract

The explosive eruption of the Hunga Tonga-Hunga Ha'apai volcano on 15 January 2022 generated atmospheric waves traveling around the Earth, which caused ionospheric disturbances on various spatio-temporal scales. A HF Doppler sounding system in Japan detected characteristic ionospheric disturbances showing periodic oscillations in the Doppler frequency with a period of ~ 4 min. In this study, such periodic oscillations were examined by comparing Doppler frequency data with Total Electron Content data obtained by Global Navigation Satellite System. The observed periodic oscillations in the Doppler frequency were characterized by a sawtooth or S-letter shaped variation, implying the passage of the traveling ionospheric disturbances through the reflection points of the HF Doppler sounding system. It was also found that the periodic oscillations occurred prior to the arrival of the tropospheric Lamb wave excited by the Tonga eruption. From the total electron content data, the traveling ionospheric disturbances causing the periodic oscillations were excited by the tropospheric Lamb waves at the conjugate point in the southern hemisphere, namely, the electric field perturbations due to the Lamb waves in the southern hemisphere mapped onto the sensing area of the HF Doppler sounding system in the northern hemisphere along the magnetic field lines. The periodic oscillations were observed only in the path between Chofu transmitter and Sarobetsu receiver, whose the radio propagation path is almost aligned in the north–south direction. This suggests that the traveling ionospheric disturbance has a structure elongating in the meridional direction. The variation in the Doppler frequency was reproduced by using a simple model of the propagation of the traveling ionospheric disturbances and the resultant motion of the reflection point. As a result, the vertical motion of the reflection point associated with the periodic oscillations was estimated to be about 1 km. It is known that 4-min period variations are sometimes observed in association with earthquakes, which is due to resonances of acoustic mode waves propagating between the ground and the lower ionosphere. Therefore, a similar resonance structure in the southern hemisphere is a plausible source of the traveling ionospheric disturbances detected in the northern hemisphere.

Keywords HF Doppler (HFD) sounding, Total electron content (TEC), Traveling ionospheric disturbances (TIDs), Volcanic eruption, S-shaped variation

*Correspondence:
Hiroyuki Nakata
nakata@faculty.chiba-u.jp
Full list of author information is available at the end of the article

Graphical Abstract

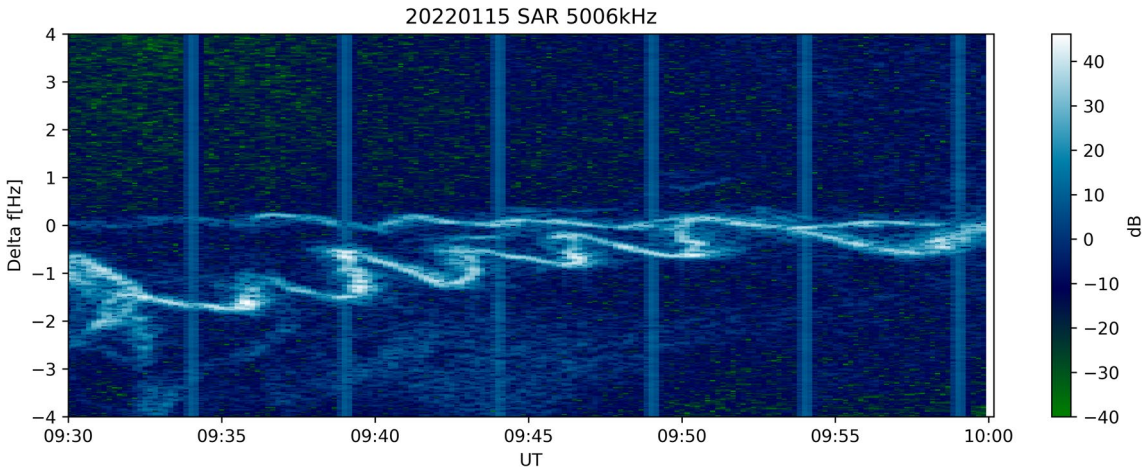

Introduction

It has been known that various large-scale natural disasters generate powerful atmospheric waves that reach the ionospheric altitudes and thus cause ionospheric disturbances (Astafyewa 2019). The eruption of the Hunga Tonga-Hunga Ha'apai volcano on January 15, 2022, was strong enough to generate atmospheric waves propagating all the way around the Earth (Matoza et al. 2022; Write et al. 2022). Disturbances caused by this eruption were observed globally by various instruments, such as Global Navigation Satellite System (GNSS) Total Electron Content (TEC) (Astafyeva et al. 2022; Chou et al. 2022; Iyemori et al. 2022; Lin et al. 2022; Saito 2022; Shinbori et al. 2022; Themens et al. 2022; Zhang et al. 2022), magnetometers (Iyemori et al. 2022; Schnepf et al. 2022; Yamazaki et al. 2022), density/wind measurements from satellites (Gasque et al. 2022; Harding et al. 2022; Liu et al. 2022; Wright et al. 2022), and ground-based infrasound observations (Chum et al. 2022; Nishikawa et al. 2022).

One of the characteristics of the ionospheric fluctuations observed during this eruption event is the occurrence of disturbances at magnetic conjugation points. Around Japan, the tropospheric Lamb wave generated by the eruption arrived at around 11 UT (Universal Time), while ionospheric fluctuations were observed a few hours earlier (at around 8 UT) (e.g., Shinbori et al. 2022). In Australia, which is the magnetic conjugate point of Japan, the tropospheric Lamb wave arrived at around 8 UT and atmospheric/ionospheric variations had been observed at the same time. It was previously reported that such magnetically conjugate ionospheric disturbances were confirmed near the epicenters of large earthquakes (Iyemori et al. 2005). In the case of the Tonga eruption, the remarkable conjugacy in the fluctuations was observed even in an area far from the volcano (e.g., Lin et al. 2022; Shinbori et al. 2022; Themens et al. 2022).

The Tonga eruption was an extremely powerful event, resulting in substantial ionospheric disturbances observed all over the earth. Most of the previous studies that examined the ionospheric disturbances associated with the Tonga eruption have focused on the variations with temporal scales extending to ten minutes or beyond. This is because finer-scale fluctuations were hidden by the large-scale disturbances and were difficult to detect. On the other hand, HF Doppler (HFD) observation enables the detection of short-period ionospheric variations around the reflection points of radio waves. In the present Tonga eruption event, we observed 4-min period Doppler frequency variations at an observatory far from the volcano, which have not been reported in previous studies. The periodic oscillations were observed at a certain pair of transmitting and receiving points, suggesting the existence of characteristic structures of ionospheric disturbances. Therefore, we have analyzed the HFD data together with the TEC data to examine the characteristics of the periodic oscillations in detail.

Data

The HFD sounding system employed in this study has been operative since 2001 by a joint effort of four research institutes in Japan. An upgrade of the observation system has been ongoing and the analog-based receivers are being replaced with newly developed digital receivers, equipped with Software-Defined Radio receivers (Nakata et al. 2021). The new HFD

sounding system utilizes radio waves at four frequencies: 5.006/8.006 MHz, both transmitted from Chofu (JG2XA), Tokyo and 3.925/6.055 MHz of Radio NIKKEI (JOZ), transmitted, respectively, from Nemuro, Hokkaido and Nagara, Chiba. The locations of the transmitters and receivers are shown in Fig. 1.

In general, the Doppler frequency data are used to estimate the vertical motion of the plasma in the ionosphere at the reflection point, which is normally located between the transmitting and receiving stations. Due to the small ionization rate in the ionosphere (less than 10^{-3}), we can assume that neutral particles dominate the motion of ionospheric plasma. Therefore, it is possible to infer the motions of neutral particles from the Doppler frequency data unless there is a significant influence from the magnetosphere.

We also made use of the TEC data obtained every 1 s in Japan and Australia. In Japan, GNSS data were obtained from the GNSS Earth Observation Network System (GEONET) operated by the Geospatial Information Authority of Japan (GSI). This dense GPS array consists of more than 1300 GPS stations, with each station recording carrier phase and pseudo-range measured at two frequencies. The GNSS data in Australia were obtained from Geoscience Australia. From these data, we derived the slant TEC, which have been converted to the vertical TEC by considering the zenith angle of the line-of-sight (LOS) between the satellite and the receiver. In this study, we assumed the altitude of the ionospheric pierce point (IPP) to be 300 km, with a mask angle of 30 degrees.

Observation results

HF Doppler observation

Figure 2(a) shows the dynamic spectrum of the radio wave at the frequency of 5.006 MHz received at the Sarobetsu (SAR) observatory for 3 h from 08:00 to 11:00 UT on January 15, 2022. The color bar shows the intensity of the radio wave. The whitish line (in fact white-blue line) in the plot traces the variation in the Doppler frequency. During two intervals, 08:40–09:10 UT and 09:30–10:20 UT, clear periodic oscillations of the Doppler frequency are observed. Figure 2(b) shows the enlarged figure of Fig. 2(a) during 09:30–10:00 UT, where sawtooth or S-shaped variations in the Doppler frequency were again recognized. Since the arrival time of the tropospheric Lamb wave excited by the eruption was ~ 11 UT in Japan (e.g., Chum et al. 2022), the periodic oscillations occurred prior to the direct arrival of the Lamb waves from the volcano. Figure 2(c) shows the 6.055 MHz data at Sarobetsu in the same format as Fig. 2(a). In this plot, the similar periodic variations in the Doppler frequency are detected during 08:40–09:00 UT. However, this observation was made near the local sunset when the electron density was decreasing. Therefore, after 09:15 UT, there was not enough electron density to reflect the radio wave at 6.055 MHz; thus, periodic oscillation was not seen in the second half of the interval. For the same reason, the radio wave at 8.006 MHz was not received at Sarobetsu during this period.

Several data from receiving stations other than Sarobetsu are summarized in Fig. 3. Although the Doppler frequencies were highly disturbed in all the panels,

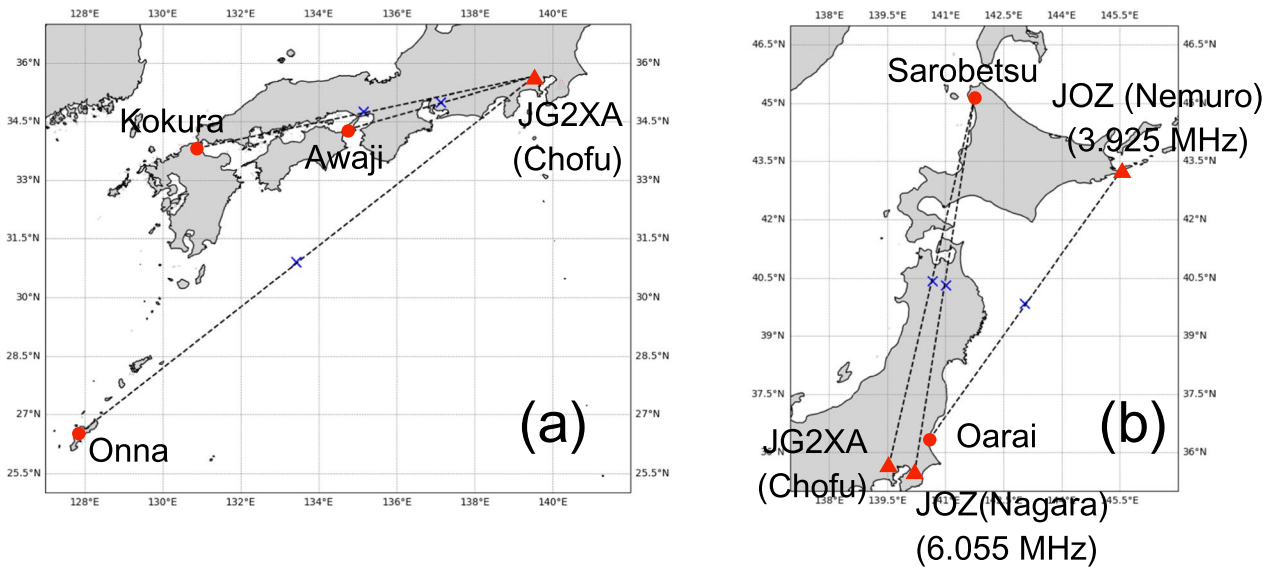

Fig. 1 The maps of Japan. The left panel (**a**) and right panel (**b**) show the western and eastern parts of Japan, respectively. The red triangles and circles show the locations of the transmitters and receivers, respectively. The crosses show the midpoints of the transmitters and receivers

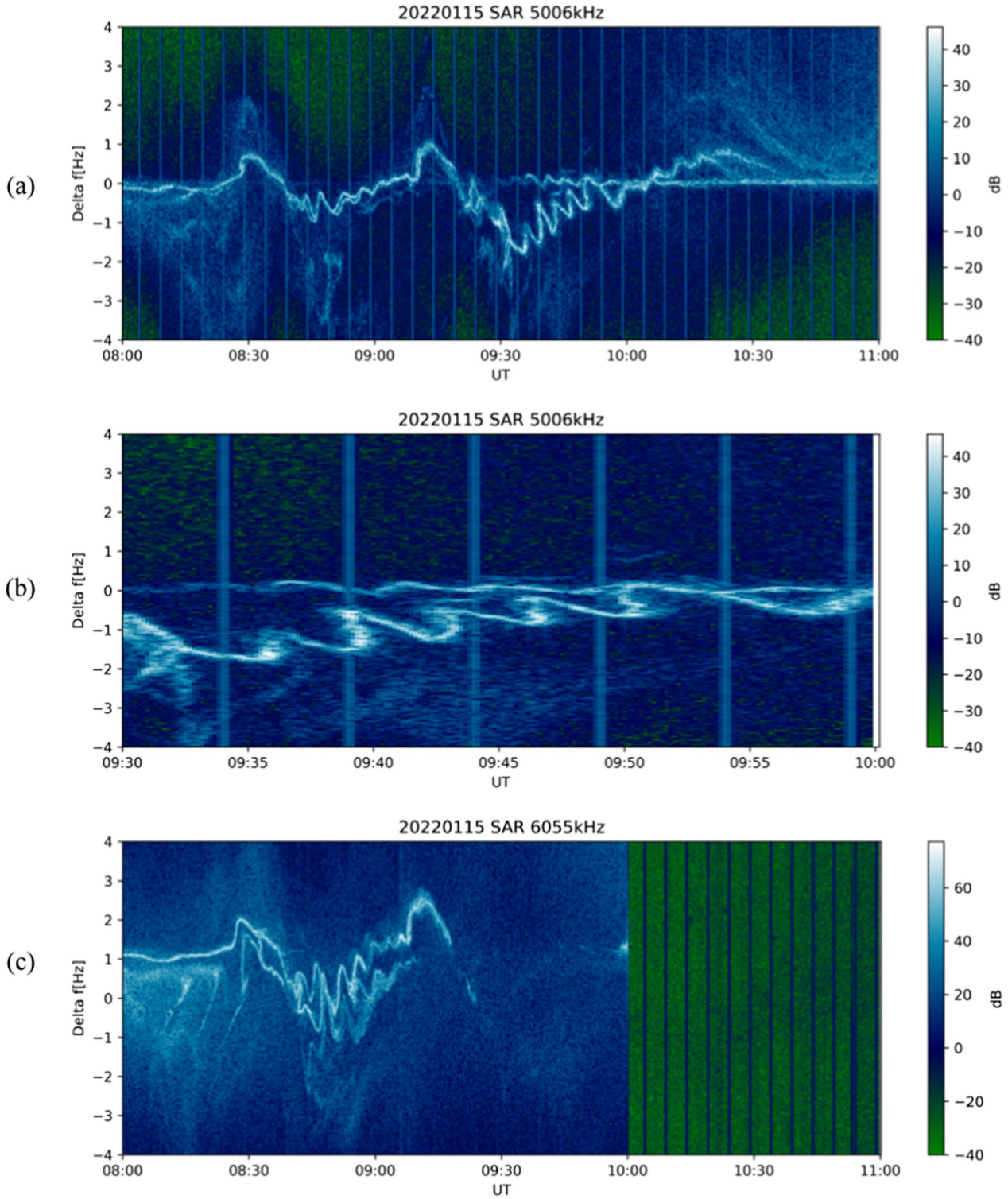

Fig. 2 The dynamic spectrums of the received radio waves observed at Sarobetsu on January 15th, 2022. The top panel (**a**) shows the dynamic spectrum at the frequency of 5006 kHz over a duration of 3 h (08:00–11:00 UT). The middle panel (**b**) is the enlarged depiction of top panel, specifically from 09:30 to 10:00 UT. The bottom panel (**c**) shows the dynamic spectrum the 6055-kHz radio wave

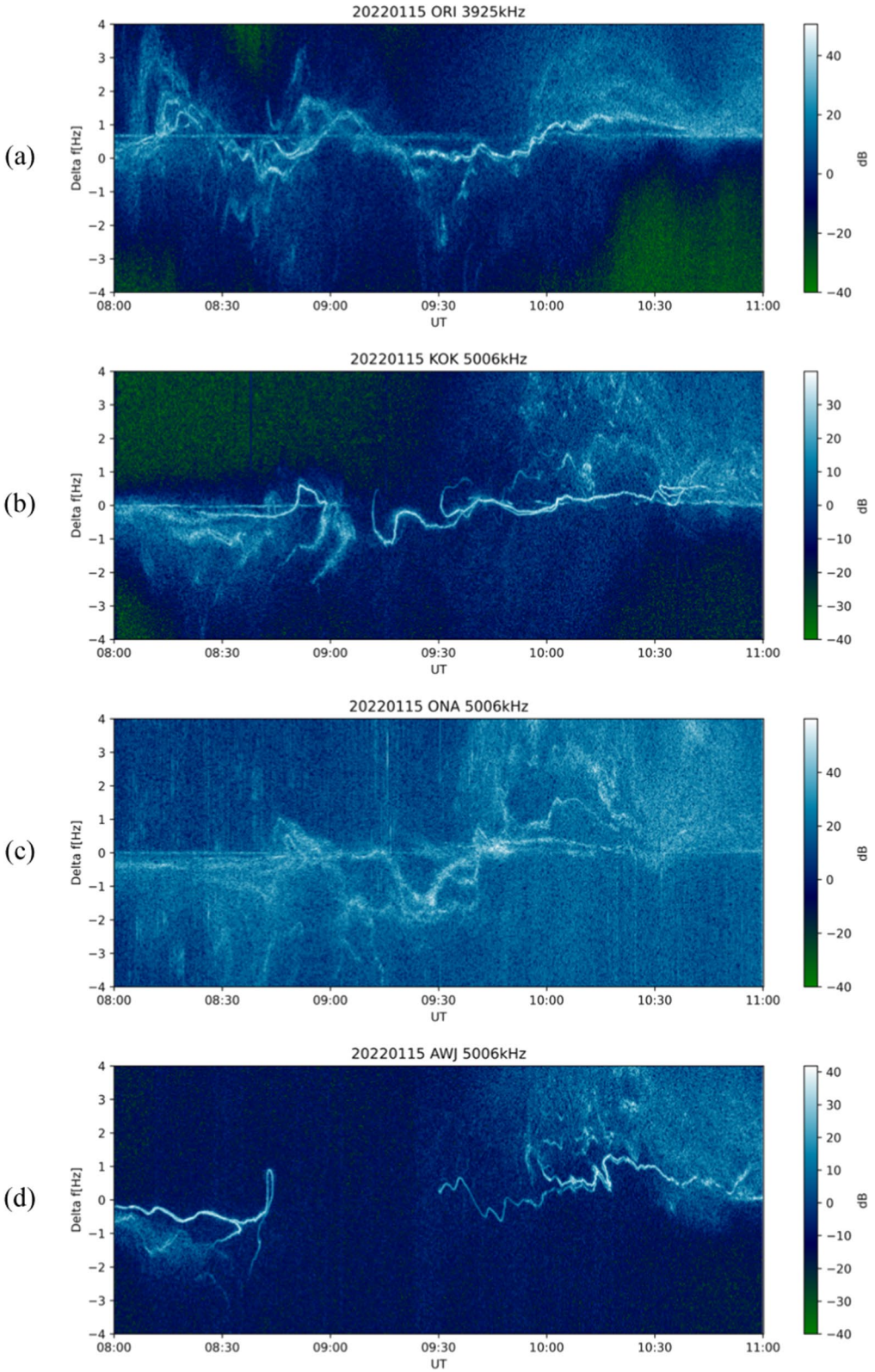

Fig. 3 The dynamic spectrums of the received radio waves for 3 h (08:00–11:00 UT) observed on January 15th, 2022. The top panel (**a**) shows the dynamic spectrum at the frequency of 3925 kHz observed at Oarai station. The other panels (**b**), (**c**) and (**d**) show the dynamic spectrums of the 5006-kHz radio wave observed at Kokura, Onna, Awaji, respectively

no clear indication of periodic oscillation was recognized. Figure 3(a) shows that the receiver at Oarai (ORI) captured several diffuse Doppler traces of the 3.925-MHz radio wave transmitted from Nemuro, Hokkaido. Although the propagation path between Nemuro and Oarai was close to the path between Chofu and Sarobetsu as depicted in Fig. 1(b), no periodic fluctuation was observed in the data from Oarai. The 5.006-MHz data from Kokura (KOK), Onna (ONA) and Awaji (AWJ), which are, respectively, plotted in the bottom three panels of Fig. 3, demonstrate that no periodic fluctuation was observed along the propagation path covering the western part of Japan. These results indicate that distinct periodic oscillations were observed only in the path between Chofu and Sarobetsu, where the propagation path was oriented in the north–south direction.

The data from Sarobetsu in Fig. 2 indicate that the periodic oscillations were seen at both the 5.006 MHz and 6.055 MHz frequencies. Since the altitudes of the reflection points of these two radio waves are different, the periodic oscillation was distributed in a certain range of altitude. This implies a possibility of detecting similar periodic variations in the TEC data; thus, TEC data over Japan and Australia have been analyzed and will be presented in the following subsection.

TEC observation

A number of previous studies reported that TEC disturbances were observed in association with the Tonga eruption. Most of such previous studies, however, have investigated longer-period fluctuations, whose period was longer than 10 min (e.g., Lin et al. 2022; Shinbori et al. 2022). Behavior of relatively shorter variations, like the one seen in the HFD data, has not yet been examined. In this study, we have employed 1-Hz sampling TEC data to identify signatures of such short-period fluctuations in both hemispheres.

First, we present the TEC data over Australia, which is the magnetically conjugate point of the sensing area of the HFD observation in Japan. Figure 4 shows the temporal variations of TEC data for a 2-h interval from 08:00 to 10:00 UT, obtained from the BULA station (22.9135°S, 139.9031°E). To extract the 4-min period (about 4.1 mHz) variation, time-series data have been derived by applying a high-pass filter with a cutoff frequency of 2.5 mHz. Note that the TEC data shown in Figs. 4(b) (Beidou-04) and 4(c) (Beidou-59) are acquired by navigation signals transmitted from BeiDou satellites in geostationary orbit. The ionospheric pierce points (IPPs) of the ray paths between BULA and three satellites (GPS-31: G-31, BeiDou-04: C-04, and BeiDou-59: C−59) at an altitude of 300 km are plotted in Fig. 5. In this figure, the blue circle shows the geomagnetically conjugate point of the sensing area of the Sarobetsu data (i.e., the midpoint of the propagation path between Chofu and Sarobetsu), which is close to the IPPs of the TEC observations.

Figure 4 shows that 4-min periodic disturbances occurred from 08:00 to 10:00 UT. In particular, the amplitudes of the periodic fluctuations increased twice in the Beidou-59 time-series, one from 08:30 to 08:50 UT and the other from 09:00 to 09:50 UT. Although the longitude of the IPP of C-59 is located slightly to the east of the conjugate point of the HFD sensing area, it is reasonable to consider that the variations of TEC in the southern hemisphere well correspond to the periodic oscillation of Doppler frequency in the northern hemisphere.

Next, we present the TEC data over Japan. Figure 6 shows plots of the temporal variations of TEC for the same 2-h interval from the tracks of the IPPs shown in Fig. 7. Because of significant noise at high frequencies, these TEC time-series data have been derived by applying a bandpass filter with a bandwidth of 3 mHz to 5 mHz. Navigation signals from geostationary satellites were not available for TEC data over Japan because the GEONET do not obtain the BeiDou data. Therefore, all the TEC data in Fig. 6 were obtained from signals of GPS satellites whose IPPs were passing through the sensing area of the HFD observation. The IPP of PRN 27 was located near the observation point between 08:30 and 09:10 UT. During this period, a 4-min period variation was enhanced in the corresponding TEC data shown in Fig. 6(c). The IPP of PRN 8 passed near the observation points between 09:30 and 10:00 UT, during which 4-min TEC disturbances were also observed (Fig. 6(a)). Although the amplitude of these TEC variation is rather small and the periodicity of the TEC variation is not always clear, the TEC data over Japan also showed some indications of similar 4-min variations when the periodic oscillation was detected by HFD. The current comparison with the TEC data indicates that the ionospheric disturbances that caused the periodic oscillation in the HFD observation were also seen in the TEC data in both of the hemisphere. These conjugacy of TEC disturbances in this event has been reported by many previous studies that examined the longer-period fluctuations. The cause of this conjugacy is the propagation of the electric field driven by E-region dynamo along the magnetic field lines. Therefore, the shorter-period disturbances also show the same conjugacy as the longer-period fluctuations.

Discussion

One of the most interesting features of the present event is the sawtooth or S-shaped variation in the Doppler frequency. Such a variation is sometimes caused by the reflection of radio waves at the sinusoidal reflecting surface in the ionosphere that is fluctuated by TID.

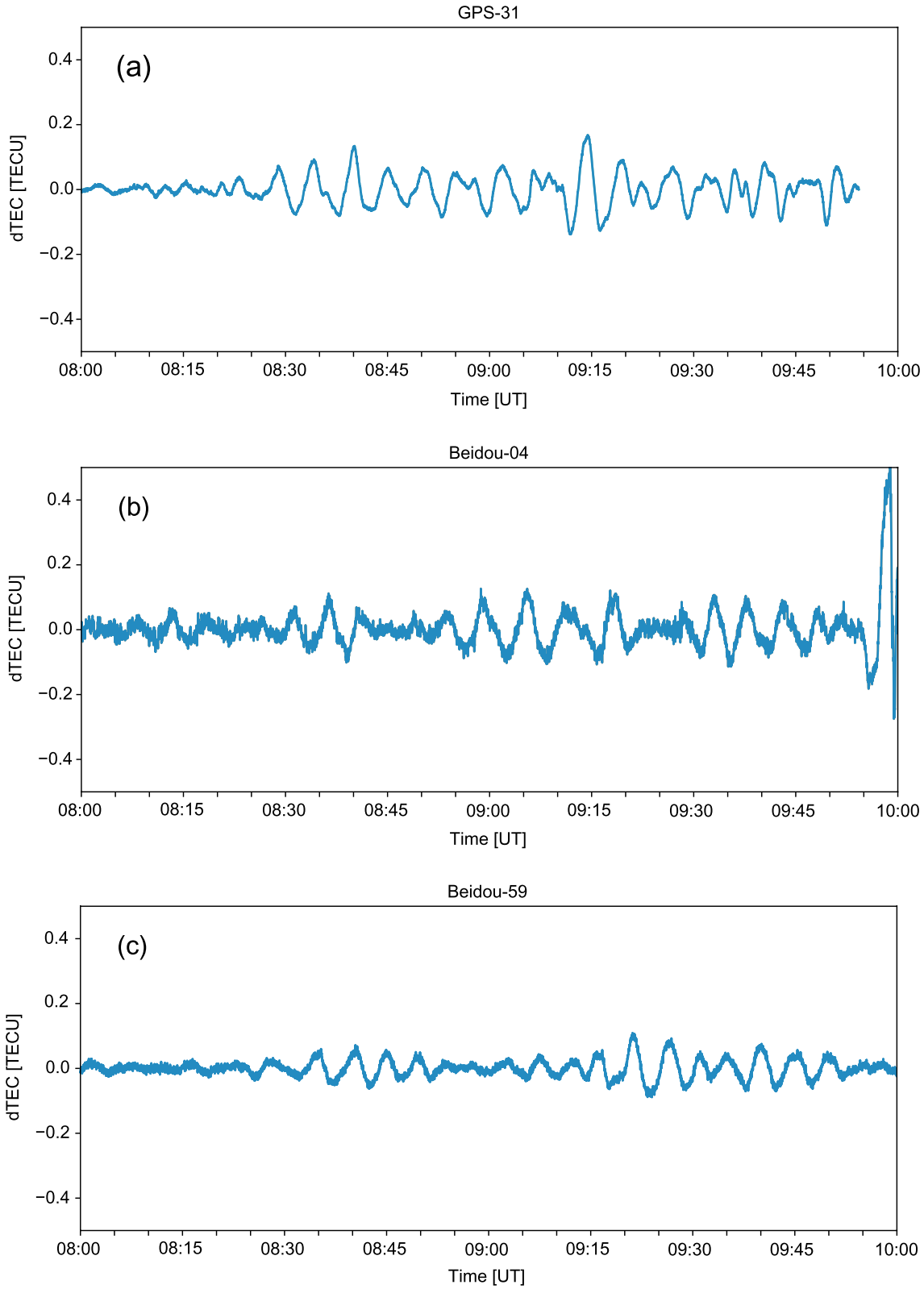

Fig. 4 The TEC data observed at BULA station in Australia. These data were derived by applying a high-pass filter with a 2.5-mHz cutoff frequency. The top panel (**a**) shows the temporal variation of TEC data observed with GPS PRN 31. The middle (**b**) panel and bottom panel (**c**) show the temporal variations of TEC observed with Beidou PRN 4 and 59, respectively

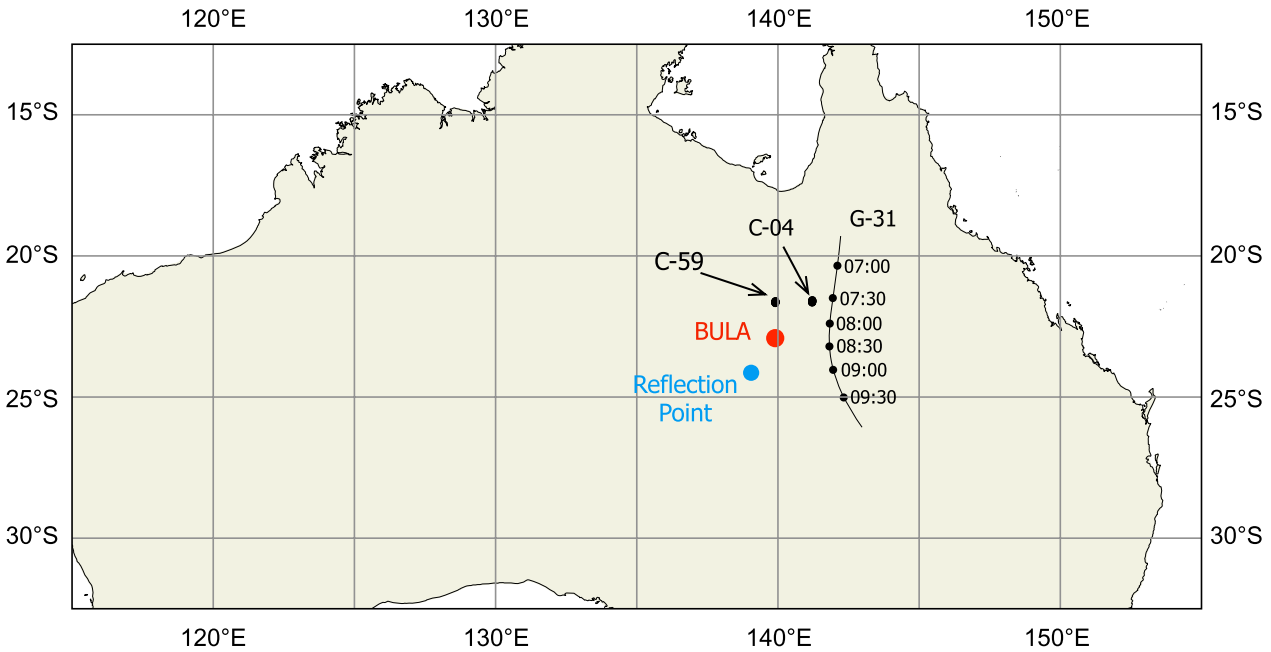

Fig. 5 A map showing the geometry of GNSS TEC measurements for satellites GPS 31 (G–31), Beidou 4 (C–04), and Beidou 59 (C–59). The red circle shows the position of BULA station. The blue circle shows the conjugate point of the midpoint between Chofu–Sarobetsu

Davies and Baker (1966) consider sinusoidal disturbances of the reflecting surface moving horizontally near the reflection point (i.e., TID passing through the observation point) and reproduced the S-shaped variations in the Doppler frequency. The schematic illustration of the relationship between TID and ray paths of radio waves is shown in Fig. 8(a). Here, a TID moving from right to left is considered whose wavy surfaces, propagating in time, are depicted by the dotted and solid lines. When the S-shaped variation is seen in the Doppler spectrogram, there are three reflection points of radio waves at the same time. This situation takes place when the ionosphere is uplifted due to fluctuations immediately above the transmitter/receiver. If the TID is moving from right to left in the figure, the Doppler frequency obtained at the reflection point on the left-hand side (the green line in the figure) is negative because this reflection point moves away from the transmitting and receiving points. Similarly, the Doppler frequency obtained by the reflection point immediately above (magenta) and on the right-hand side (purple) of the transmitting and receiving points are zero and positive, respectively. In the present event, the distance between the transmitting and receiving points is about 1000 km apart. Therefore, it is possible to assume that the wavefront of the TID extended in the north–south direction and was parallel to the propagation path of the radio wave, as shown in Fig. 8(b). TEC observations show that ionospheric disturbances over Japan propagated almost in the east–west direction (Saito 2022); thus, it is quite natural to consider that the wavefronts extending from north to south propagated from east to west. By performing a simple model calculation, we estimated the Doppler frequency variation when such a disturbance occurs. In this model calculation, the period and propagation velocity of the disturbance were set to 240 s and 250 m/s, respectively. Based on these parameters, the wavelength was also set to 60 km. The altitude of the reflected radio waves was estimated to be 244 km using the ray tracing calculation. The reproduced Doppler frequency variation is shown in Fig. 9 for a case where the uplift and downlift of the ionosphere are assumed to be ± 1 km is shown in Fig. 9. As can be seen from this figure, the Doppler frequency variation was ± 0.4 Hz. The observed results in Fig. 2 show that the magnitude of the Doppler frequency variation is about ± 0.5 Hz, although it depends on the period, which is consistent with the frequency variation estimated by the simple model.

Figure 2(a) shows not only the periodic variations, but also large increases in Doppler frequency at 08:30 and 09:15 UT. Figure 10 shows the TEC data derived by applying a high-pass filter with a 1-mHz cutoff frequency. This data was obtained along the track of the IPP of PRN 8. In this data, there are large enhancements in TEC at 08:40 and 09:20 UT. In the present event, the volcano erupted not once but multiple times. Using TEC data obtained in the vicinity of the volcano, Astafyeva et al. (2022) confirmed that at least five explosions occurred.

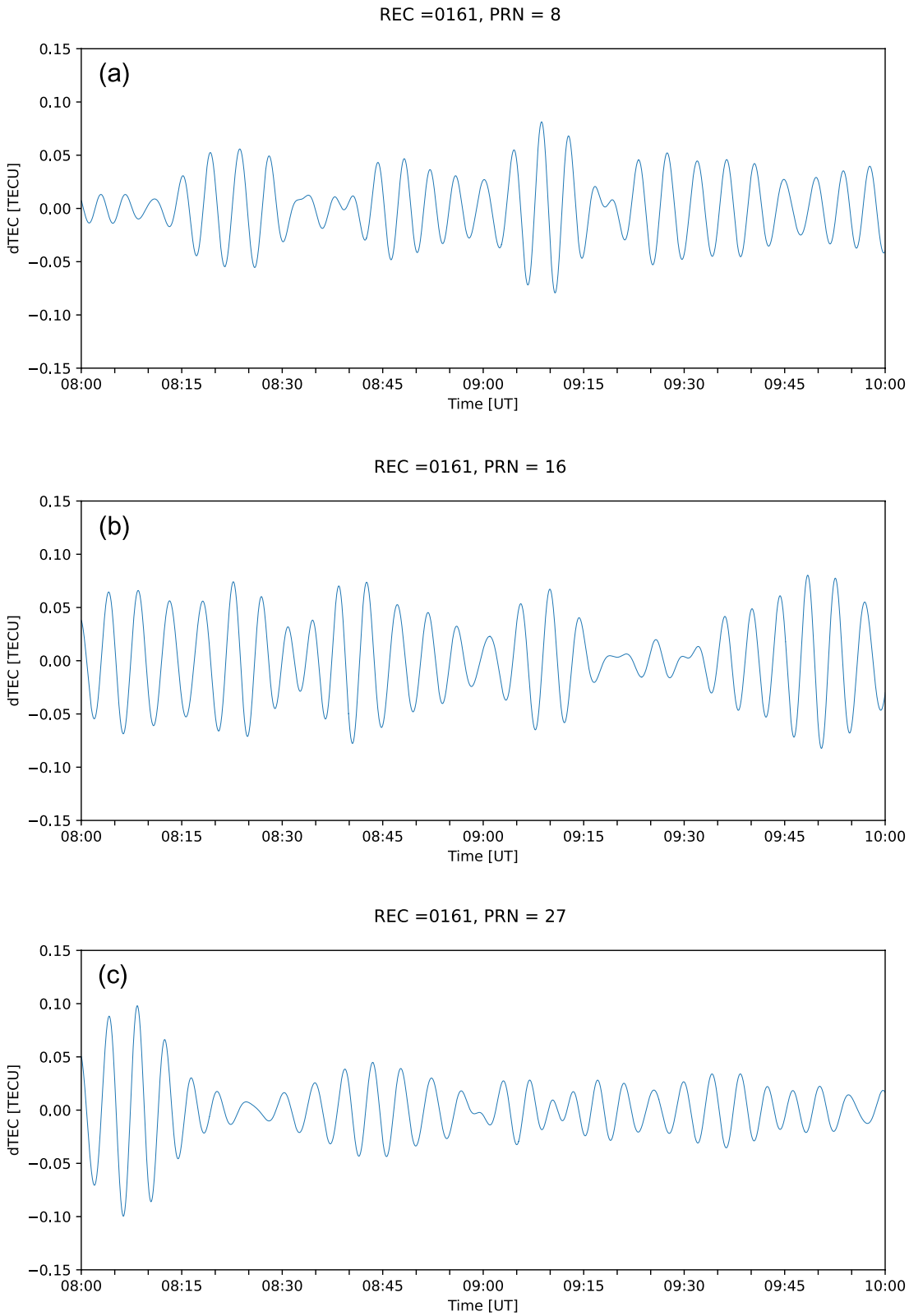

Fig. 6 The TEC data observed at a GEONET station in Japan. These data were derived by applying a bandpass filter with a bandwidth of 3 mHz to 5 mHz. The top (**a**), middle (**b**) and bottom (**c**) panels show the temporal variations of TEC observed with GPS PRN 8, 16, and 27, respectively

Fig. 7 A map showing the geometry of GNSS TEC measurements for GPS PRN8, PRN16, and PRN27. The red circle shows the position of GNSS receiver (0161). The black circles show the reflection points of the mid points between the transmitters and receivers

From the enhancements of the TEC, these enhancements of TEC were due to the second and third eruptions of the volcano. As shown in Fig. 2(a), the increases in Doppler frequency reached their maximum at 08:30 and 09:15 UT, and these timings are slightly earlier than 08:40 and 09:20 UT, when the TEC reaches its maximum. Since an increase in Doppler frequency indicates downward motion of the reflection point, both the enhancements of the Doppler frequency are consistent with those of TEC.

It is known that the 4-min oscillations are observed around epicenters of large earthquakes (Choosakul et al. 2009; Saito et al. 2011). This is because the acoustic resonance structure is formed between the ground and the lower ionosphere (Tahira 1995; Saito et al. 2011; Matsumura et al.2011). In the Tonga eruption event, this resonance was also formed near the volcano and the magnetic disturbances were observed around the volcano and its conjugate area (Iyemori et al. 2022; Yamazaki et al.

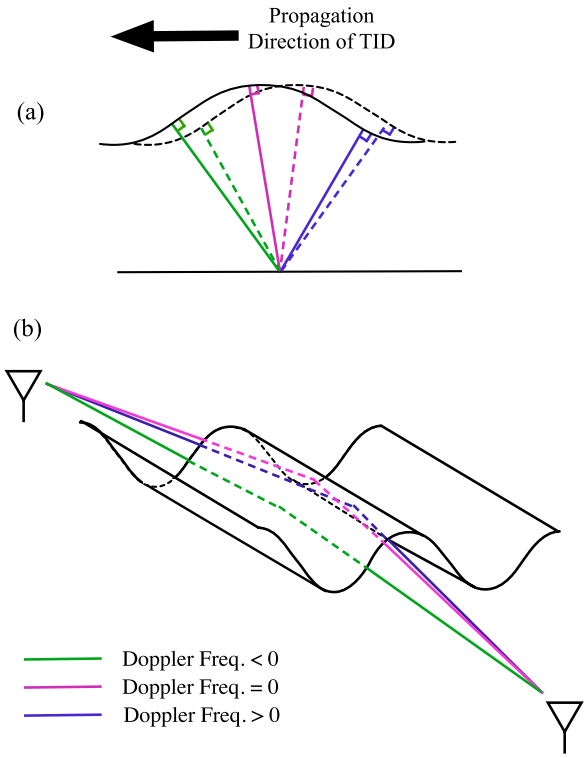

Fig. 8 The schematic figure of the traveling ionospheric disturbance and the ray paths of the radio waves. The top panel (**a**) shows the TID and the raypath of the radio waves. The bottom panel (**b**) shows a bird's-eye view of the iso-contour of the ionospheric electron density and the ray paths of the radio waves between Chofu and Sarobetsu

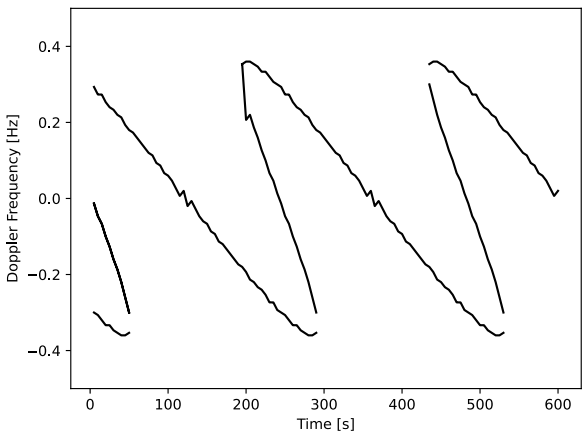

Fig. 9 The estimated Doppler shift frequency in the present event assuming that the vertical motion of the reflection point is ± 1 km

2022). The results of the present study imply that a similar resonance structure was formed far from the volcano. As for the horizontal extent of this resonance structure, Yamazaki et al. (2022) reported that the magnetic field oscillations with a period of 4 min were observed within 835 km of the volcano. The amplitude of the magnetic oscillation was about 3 nT in the vicinity of the volcano. According to Zettergren and Snively (2019), the drift velocity of ions in the ionosphere to produce magnetic field variations of a few nT on the ground amounts to several hundred m/s. In contrast, in our model calculations of the Doppler frequency variations as shown in Fig. 9, the maximum vertical velocity of the reflection point above Japan was about 8 m/s. This value is quite small to generate magnetic field disturbances on the ground even though the ionospheric variations in the present event were larger in the southern hemisphere (Shinbori et al. 2022; Yamazaki et al. 2022). The results of this paper are attributed to the fact that the HF Doppler observations capture much smaller ionospheric variations than other observations. It is noteworthy that the periodic oscillations occur shortly after these impulsive variations in Doppler frequency. The GAIA (Ground-to-topside model of Atmosphere and Ionosphere for Aeronomy) model, which is the numerical self-consistent atmosphere–ionosphere model (Jin et al. 2012), is presently employed to analyze the ionospheric variations associated with the Tonga eruption. The analysis considering atmospheric motions under non-hydrostatic equilibrium reveals the occurrence of the vertical oscillations of the ionosphere subsequent to the passage of the Lamb wave (Shinagawa, private communication). This oscillation could be attributed to the resonance between the Earth's surface and the lower ionosphere. This outcome suggests that the periodic oscillations in Doppler frequency examined in this study were a consequence of the acoustic resonance prevailing in the southern hemisphere. While more detailed analysis is anticipated in subsequent studies, this study offers observational evidence of the acoustic resonance between the Earth's surface and the lower ionosphere or similar structure far from the volcano.

Summary

Periodic oscillations of the Doppler frequency with a period of ~ 4 min were observed in association with the Tonga eruption occurred in January 2022, employing the HFD sounding system. Examination of TEC data in the northern and southern hemispheres revealed that TEC in both the hemispheres were similarly perturbed with the aforementioned periodic oscillations. These oscillations arise from the ionospheric disturbances caused by tropospheric Lamb waves in the southern hemisphere. Consequently, these disturbances lead to TID in the northern hemisphere, facilitated by the electric field propagating along the magnetic field lines. The periodic oscillations of the Doppler frequency were observed only in the path of the radio wave between Chofu and Sarobetsu, which

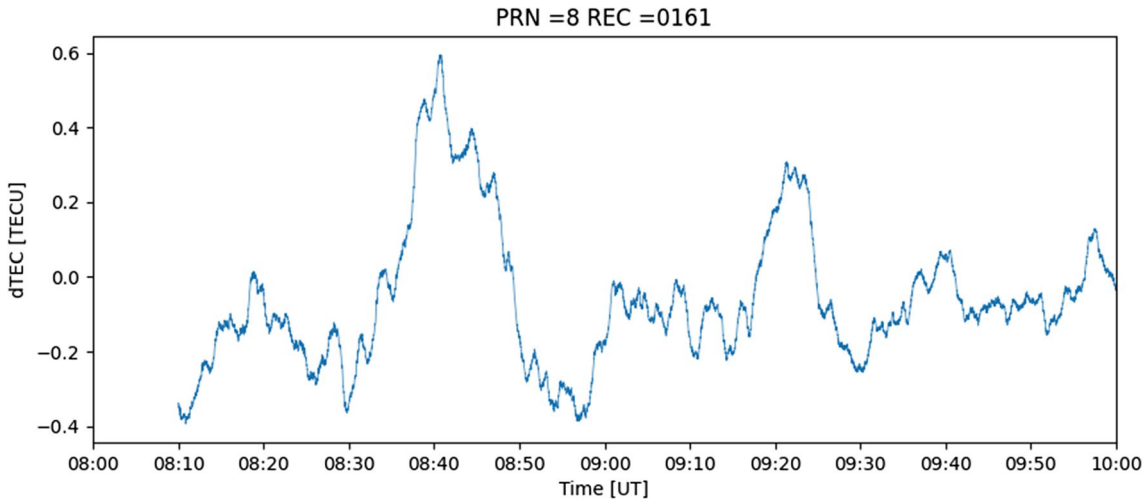

Fig. 10 The TEC time-series data obtained in the pair of the GEONET receiver No. 0161 and GPS PRN 8. This time-series data were derived by applying a high-pass filter with a 1-mHz cutoff frequency

aligns itself in a north–south direction. This result suggests that the TID has an elongating structure in the meridional direction. The estimated variation in the reflection altitude of the radio wave was approximately 1 km, which in turn generated a Doppler frequency variation almost equivalent to the observed measurements. Notably, not only periodic oscillations but also abrupt increases in Doppler frequency were detected through HFD sounding system. Moreover, these increases were observed slightly prior to the corresponding increases in TEC, thereby indicating that the enhancement of the ionospheric electron density caused the variations in Doppler frequency. The results of the present study provide the observational evidence of the occurrence of the acoustic resonance far from the volcano. The periodic oscillations examined in this study were observed since the HF Doppler sounding can detect relatively small fluctuations at reflection points of the radio waves with high accuracy. In addition, the observation network that was constructed over the entire of Japan led to results that suggest the existence of a structure extending from north to south. The present result is the case in which 4-min variations were observed at a distance from the volcano. This study offers observational evidence of the resonance structure between the Earth's surface and the lower ionosphere far from the volcano.

Abbreviations

GAIA	Ground-to-topside model of atmosphere and ionosphere for aeronomy
GEONET	GNSS Earth Observation NETwork System
GNSS	Global Navigation Satellite System
GPS	Global Positioning System
HF	High-frequency
HFD	HF Doppler
IPP	Ionospheric pierce point
TEC	Total electron content
TECU	TEC unit
TID	Traveling ionospheric disturbance
UT	Universal time

Acknowledgements
We thank Dr. Yosuke Yamazaki and the anonymous reviewer for assessing this manuscript. We also thank Dr. Hiroyuki Shinagawa for fruitful discussion on the GAIA results. We used the GNSS data provided by the GEONET and Geoscience Australia to calculate TEC data in Japan and Australia, respectively.

Author contributions
HN conducted the current research and prepared the manuscript. KH is leading a project for HFD observation in Japan and discussed the results of the measurements. SS and YO provided TEC data in Japan and Australia, respectively, and discussed the results of the TEC measurements. IT discussed the interpretation of HFD data in the event of TID. All authors read and approved the final manuscript.

Funding
YO is supported by JSPS KAKENHI Grant Number 22K21345, JSPS Bilateral Joint Research Projects No. JPJSBP120226504, and JSPS Core-to-Core Program, B. Asia-Africa Science Platforms.

Availability of data and materials
Data of the HFD sounding system in Japan and the source code for the receiver are both available at http://gwave.cei.uec.ac.jp/~hfd/. GPS-TEC data was derived from the carrier phase and pseudo-range data obtained by GNSS Earth Observation Network (GEONET). (https://www.gsi.go.jp/ENGLISH/geonet_english.html). The TEC data in Australia were derived from GNSS data obtained from Geoscience Australia (http://www.ga.gov.au/scientific-topics/positioning-navigation/geodesy/gnss-networks/data-and-site-logs).

Declarations

Ethics approval and consent to participate
Not applicable.

Consent for publication
Not applicable.

Competing interests
The authors declare that they have no competing interests.

Author details
[1]Graduate School of Engineering, Chiba University, Chiba, Japan. [2]The University of Electro-Communications, Tokyo, Japan. [3]Electronic Navigation Research Institute, National Institute of Maritime, Port and Aviation Technology, Tokyo, Japan. [4]Nagoya University, Nagoya, Japan.

Received: 31 May 2023 Accepted: 27 September 2023
Published online: 10 October 2023

References

Astafyeva E (2019) Ionospheric detection of natural hazards. Rev Geophys 57:1265–1288. https://doi.org/10.1029/2019rg000668
Astafyeva E, Maletckii B, Mikesell TD et al (2022) The 15 January 2022 Hunga Tonga eruption history as inferred from ionospheric observations. Geophys Res Lett. https://doi.org/10.1029/2022gl098827
Choosakul N, Saito A, Iyemori T, Hashizume M (2009) Excitation of 4-min periodic ionospheric variations following the great Sumatra-Andaman earthquake in 2004. J Geophys Res 114:A10313. https://doi.org/10.1029/2008ja013915
Chou M, Yue J, Lin CCH et al (2022) Conjugate effect of the 2011 Tohoku reflected tsunami-driven gravity waves in the ionosphere. Geophys Res Lett. https://doi.org/10.1029/2021gl097170
Chum J, Šindelářová T, Knížová PK et al (2022) Atmospheric and ionospheric waves induced by the Hunga eruption on 15 January 2022 Doppler sounding and infrasound. J Int Geophys. https://doi.org/10.1093/gji/ggac517
Davies K, Baker DM (1966) On frequency variations of lonospherically propagated HF radio signals. Radio Sci 1:545–556. https://doi.org/10.1002/rds196615545
Gasque LC, Wu Y, Harding BJ et al (2022) Rapid volcanic modification of the E-region dynamo: ICON's first glimpse of the Tonga eruption. Geophys Res Lett. https://doi.org/10.1029/2022gl100825
Harding BJ, Wu YJ, Alken P et al (2022) Impacts of the January 2022 Tonga volcanic eruption on the ionospheric dynamo: ICON-MIGHTI and Swarm observations of extreme neutral winds and currents. Geophys Res Lett. https://doi.org/10.1029/2022gl098577
Iyemori T, Nose M, Han D et al (2005) Geomagnetic pulsations caused by the Sumatra earthquake on December 26, 2004. Geophys Res Lett. https://doi.org/10.1029/2005gl024083
Iyemori T, Nishioka M, Otsuka Y, Shinbori A (2022) A confirmation of vertical acoustic resonance and field-aligned current generation just after the 2022 Hunga Tonga Hunga Ha'apai volcanic eruption. Earth Planets Space 74:103. https://doi.org/10.1186/s40623-022-01653-y
Jin H, Miyoshi Y, Pancheva D, Mukhtarov P, Fujiwara H, Shinagawa H (2012) Response of migrating tides to the stratospheric sudden warming in 2009 and their effects on the ionosphere studied by a whole atmosphere-ionosphere model GAIA with COSMIC and TIMED/SABER observations. J Geophys Res 117:A10323. https://doi.org/10.1029/2012JA017650
Lin J, Rajesh PK, Lin CCH et al (2022) Rapid conjugate appearance of the giant ionospheric lamb wave signatures in the northern hemisphere after Hunga-Tonga volcano eruptions. Geophys Res Lett. https://doi.org/10.1029/2022gl098222
Liu X, Xu J, Yue J, Kogure M (2022) Strong gravity waves associated with Tonga volcano eruption revealed by SABER observations. Geophys Res Lett. https://doi.org/10.1029/2022gl098339
Matoza RS, Fee D, Assink JD et al (2022) Atmospheric waves and global seismoacoustic observations of the January 2022 Hunga eruption Tonga. Science. https://doi.org/10.1126/science.abo7063
Matsumura M, Saito A, Iyemori T et al (2011) Numerical simulations of atmospheric waves excited by the 2011 off the Pacific coast of Tohoku Earthquake. Earth Planets Space 63:68. https://doi.org/10.5047/eps.2011.07.015
Nakata H, Nozaki K, Oki Y et al (2021) Software-defined radio-based HF doppler receiving system. Earth Planets Space. https://doi.org/10.1186/s40623-021-01547-5
Nishikawa Y, Yamamoto M, Nakajima K et al (2022) Observation and simulation of atmospheric gravity waves exciting subsequent tsunami along the coastline of Japan after Tonga explosion event. Sci Rep-Uk 12:22354. https://doi.org/10.1038/s41598-022-25854-3
Saito S (2022) Ionospheric disturbances observed over Japan following the eruption of Hunga Tonga-Hunga Ha'apai on 15 January 2022. Earth Planets Space 74:57. https://doi.org/10.1186/s40623-022-01619-0
Saito A, Tsugawa T, Otsuka Y et al (2011) Acoustic resonance and plasma depletion detected by GPS total electron content observation after the 2011 off the Pacific coast of Tohoku Earthquake. Earth Planets Space 63:64. https://doi.org/10.5047/eps.2011.06.034
Schnepf NR, Minami T, Toh H, Nair MC (2022) Magnetic signatures of the 15 January 2022 Hunga Tonga-Hunga Ha'apai volcanic eruption. Geophys Res Lett. https://doi.org/10.1029/2022gl098454
Shinbori A, Otsuka Y, Sori T et al (2022) Electromagnetic conjugacy of ionospheric disturbances after the 2022 Hunga Tonga-Hunga Ha'apai volcanic eruption as seen in GNSS-TEC and SuperDARN Hokkaido pair of radars observations. Earth Planets Space 74:106. https://doi.org/10.1186/s40623-022-01665-8
Tahira M (1995) Acoustic resonance of the atmospheric at 3.7 Hz. J Atmos Sci 52:2670–2674
Themens DR, Watson C, Žagar N et al (2022) Global propagation of ionospheric disturbances associated with the 2022 Tonga volcanic eruption. Geophys Res Lett. https://doi.org/10.1029/2022gl098158
Wright CJ, Hindley NP, Alexander MJ et al (2022) Surface-to-space atmospheric waves from Hunga Tonga-Hunga Ha'apai eruption. Nature 609:741–746. https://doi.org/10.1038/s41586-022-05012-5
Yamazaki Y, Soares G, Matzka J (2022) Geomagnetic detection of the atmospheric acoustic resonance at 3.8 mHz during the Hunga Tonga eruption event on 15 January 2022. J Geophys Res Space Phys. https://doi.org/10.1029/2022ja030540
Zettergren MD, Snively JB (2019) Latitude and longitude dependence of ionospheric TEC and magnetic perturbations from infrasonic-acoustic waves generated by strong seismic events. Geophys Res Lett 46:1132–1140. https://doi.org/10.1029/2018gl081569
Zhang S-R, Vierinen J, Aa E et al (2022) 2022 Tonga volcanic eruption induced global propagation of ionospheric disturbances via lamb waves. Frontiers Astronomy Space Sci 9:871275. https://doi.org/10.3389/fspas.2022.871275

Publisher's Note